



Arabidopsis FNRL protein is an NADPH-dependent chloroplast oxidoreductase resembling bacterial ferredoxin-NADP⁺ reductases

Journal:	<i>Physiologia Plantarum</i>
Manuscript ID	PPL-2017-00256
Manuscript Type:	Special Issue article
Date Submitted by the Author:	31-Jul-2017
Complete List of Authors:	<p>Koskela, Minna; University of Turku, Department of Biochemistry/Molecular Plant Biology Dahlström, Käthe; Åbo Akademi University, Department of Biosciences Goni, Guillermina; University of Zaragoza, Department of Biochemistry and Molecular and Cellular Biology Lehtimäki, Nina; Turun Yliopisto, Department of Biochemistry Nurmi, Markus; University of Turku, Department of Biochemistry Velázquez-Campoy, Adrián; University of Zaragoza, Department of Biochemistry and Molecular and Cellular Biology; Fundación ARAID, Diputación General de Aragón Hanke, Guy; Queen Mary University of London, School of Biological and Chemical Sciences Bölter, Bettina; Ludwig-Maximilians-Universität München Fakultät für Biologie, 5Department of Biology I Salminen, Tiina; Åbo Akademi University, Department of Biosciences Medina, Milagros; University of Zaragoza, Department of Biochemistry and Molecular and Cellular Biology Mulo, Paula; University of Turku, Department of Biochemistry</p>
Key Words:	chloroplast, electron transfer, flavoenzyme, oxidoreductase, structural model

1
2
3
4
5
6
7
8
9
10
11
12
13
14
15
16
17
18
19
20
21
22
23
24
25
26
27
28
29
30
31
32
33
34
35
36
37
38
39
40
41
42
43
44
45
46
47
48
49
50
51
52
53
54
55
56
57
58
59
60

***Arabidopsis* FNRL protein is an NADPH-dependent chloroplast
oxidoreductase resembling bacterial ferredoxin-NADP⁺ reductases**

Minna M. Koskela¹, Käthe M. Dahlström^{2#}, Guillermina Goñi³, Nina Lehtimäki¹, Markus Nurmi^{1§}, Adrian Velazquez-Campoy^{3,4}, Guy Hanke⁵, Bettina Bölter⁶, Tiina A. Salminen², Milagros Medina^{*3} and Paula Mulo^{*1}

¹Molecular Plant Biology, Department of Biochemistry, University of Turku, Turku, Finland

²Structural Bioinformatics Laboratory, Biochemistry, Faculty of Science and Engineering, Åbo Akademi University, Turku, Finland

³Department of Biochemistry and Molecular and Cellular Biology, Faculty of Sciences and Institute of Biocomputation and Physics of Complex Systems (BIFI-IQFR and GBsC-CSIC Joint Units), University of Zaragoza, Spain

⁴Fundación ARAID, Diputación General de Aragón, Spain

⁵School of Biochemistry and Chemistry, Queen Mary University of London, United Kingdom

⁶Department of Biology I, Botany, Ludwig-Maximilians-Universität München, Planegg-Martinsried, Germany

[#]Current address: Institute of Chemistry, University of Campinas (UNICAMP), Campinas, SP, Brazil

[§]Current address: Max Planck Institute of Molecular Plant Physiology, Potsdam, Brandenburg, Germany

*shared corresponding authorship: Paula Mulo (pmulo@utu.fi) and Milagros Medina (mmedina@unizar.es)

Abstract

Plastidic ferredoxin-NADP⁺ oxidoreductases (FNRs; EC:1.18.1.2) together with bacterial type FNRs (FPRs) form the plant-type FNR family. Members of this group contain a two-domain scaffold that forms the basis of an extended superfamily of FAD dependent oxidoreductases. In the present study, we show that the *Arabidopsis thaliana* At1g15140 (FERREDOXIN-NADP⁺ OXIDOREDUCTASE - LIKE, FNRL) is an FAD-containing NADPH dependent oxidoreductase present in the chloroplast stroma. Determination of the kinetic parameters using the DCPIP NADPH-dependent diaphorase assay revealed that the reaction catalysed by a recombinant FNRL protein followed a saturation Michaelis-Menten profile on the NADPH concentration with $k_{\text{cat}} = 3.24 \pm 0.17 \text{ s}^{-1}$, $K_m^{\text{NADPH}} = 1.6 \pm 0.3 \text{ }\mu\text{M}$ and $k_{\text{cat}} / K_m^{\text{NADPH}} = 2.0 \pm 0.4 \text{ }\mu\text{M}^{-1} \text{ s}^{-1}$. Biochemical assays suggested that FNRL is not likely to interact with *Arabidopsis* ferredoxin 1 (AtFd1), which is supported by the sequence analysis implying that the known Fd-binding residues in plastidic FNRs differ from those of FNRL. Additionally, based on structural modelling FNRL has an FAD-binding N-terminal domain built from a six-stranded β -sheet and one α -helix, and a C-terminal NADP⁺-binding α/β domain with a five-stranded β -sheet with a pair of α -helices on each side. The FAD-binding site is highly hydrophobic and predicted to bind FAD in a bent conformation typically seen in bacterial FPRs.

Abbreviations

CD, circular dichroism; CTC, charge-transfer complexes; DCPIP, 2,6-dichlorophenolindophenol; FAD, flavin adenine dinucleotide; FMN, flavin mononucleotide; Fd, ferredoxin; FNR, ferredoxin NADP⁺ oxidoreductase; FNRL, At1g15140 FNR-like; HT, hydride transfer; LFNR, leaf-type ferredoxin NADP⁺ oxidoreductase; ITC, isothermal titration calorimetry; ox, oxidized; red, reduced;

Introduction

Flavoproteins and flavoenzymes contain a flavin adenine dinucleotide (FAD) or a flavin mononucleotide (FMN) cofactor that is usually a key to the proteins function. Flavoproteins are involved in a wide range of biological processes in all kingdoms of life. In plants, they play crucial roles in mediating light responses, such as phototropism and development, motility of cell organelles, stress responses, photosynthetic reactions and regulation of circadian rhythm (Conrad et al. 2014). Despite their important roles in plant metabolism, the function of a number of plant flavoenzymes has remained unexplored to date.

Chloroplast ferredoxin-NADP⁺ oxidoreductases (FNRs) together with bacterial type FNRs (FPRs) form the plant-type FNR family (Aliverti et al. 2008, Ceccarelli et al. 2004). These proteins contain a two-domain scaffold, which forms the basis of an extended superfamily of oxidoreductases (Karplus et al. 1991, Serre et al. 1996). FNR is a widely studied chloroplast flavoenzyme that catalyses the last step of linear photosynthetic electron transfer by oxidizing ferredoxin (Fd) and reducing NADP⁺ to NADPH ($2\text{Fd}_{\text{rd}} + \text{NADP}^+ \rightarrow 2\text{Fd}_{\text{ox}} + \text{NADPH}$) (Arnon 1991), reviewed in (Mulo and Medina 2017). NADPH, in turn, is mainly used in assimilation of carbon and other biosynthetic pathways. On the contrary, FPRs reduce Fds or flavodoxins, providing electrons to a number of reactions ranging from amino acid and nucleotide metabolism to assimilation of nitrogen and responses to oxidative stress (Ceccarelli et al. 2004).

All plant species studied thus far contain a small family of *FNR* genes. The isoforms can be classified into two groups. The first group is composed of photosynthetic or leaf-type (LFNR) FNRs, which function in photosynthesis and are located in chloroplasts. The second group is composed of heterotrophic or root-type FNRs, which apparently catalyze NADPH oxidation and Fd reduction in non-photosynthetic plastids (e.g. in roots). Both classes contain (at least) two distinct forms. For instance, the chloroplasts of *Arabidopsis thaliana* possess two forms of LFNRs, LFNR1 and LFNR2, which show partially redundant functions (Hanke et al. 2005, Lintala et al. 2007, 2009).

The N-terminal domain of plant-type FNRs, which contains six antiparallel β strands organized in two perpendicular β sheets, is responsible for FAD binding, while the C-terminal domain, consisting of five parallel β strands surrounded by seven α helices, binds NADP⁺ (Serre et al. 1996). FAD binds outside the antiparallel β barrel of FNR, and Fd in a cleft between the FAD- and NADP⁺-domains by interacting with the basic amino acid residues of FNR, through hydrogen bonds, van der Waals forces and hydrophobic interactions (Jelesarov et al. 1993, Mulo and Medina 2017). The binding site for FAD is the same in FNRs and FPRs, but they bind FAD in extended and bent conformations, respectively. The extended FAD conformation is bound by the β -hairpin structure after $\beta 5$ in FNRs (Musumeci et al. 2011, Serre et al. 1996), which is replaced by a short loop in bacterial FPRs. In

1
2
3 FPRs, the bent conformation of FAD also enables stacking of the adenosine ring with a C-terminal
4 aromatic residue (Aliverti et al. 2008, Ceccarelli et al. 2004).
5

6
7 In the present study, we have explored the structure of *Arabidopsis thaliana* At1g15140 (hereafter
8 FERREDOXIN-NADP⁺ OXIDOREDUCTASE-LIKE, FNRL), annotated as an FAD/NAD(P)-
9 binding oxidoreductase in TAIR (<https://www.arabidopsis.org/>), to compare its properties with those
10 of other FNR proteins. Characterization of the recombinant protein revealed that FNRL is an active
11 FAD-containing NADPH dependent oxidoreductase, and structural modelling indicated that it
12 resembles bacterial FPRs more than plastid FNRs.
13
14
15

16 17 18 **Materials and methods**

19 *Sequence analysis and structural modelling*

20 The sequence for FNRL from UniProtKB (accession code Q9XI55) was used for domain analysis
21 with Simple Modular Architecture Research Tool (SMART) (Letunic et al. 2015, Schultz et al. 1998),
22 InterPro (Finn et al. 2017, Jones et al. 2014) and PROSITE (de Castro et al. 2006), as well as for
23 secondary structure predictions with PsiPred (Jones 1999, McGuffin et al. 2000) and to search the
24 Protein Data Bank for crystal structures to be used as templates with PSI-BLAST at NCBI. Hits with
25 significant E-value (< 0.001) and query coverage > 60 % (PDB accession codes 4WQM[A] [Acheson
26 et al., 2015], 1QFJ[A] [Ingelman et al., 1999], 2R6H[C] [Kim et al., to be published], 3FPK[A] [Kim
27 et al., to be published] and 2XNJ[A] [Musumeci et al., 2011]) were superimposed with VERTAA
28 (Johnson and Lehtonen, 2000) in the BODIL modelling environment (Lehtonen et al. 2004) to
29 generate a structure-based alignment, to which the FNRL sequence was aligned. The structure of pea
30 (*Pisum sativum*) (PDB accession code 1QG0[A]) (Deng et al., 1999) was also superimposed on the
31 bacterial crystal structures to aid the correct alignment of the full-length sequences for pea leaf FNR
32 and root and leaf FNR from maize (*Zea mays*) and *A. thaliana* using pre-aligned sequences in
33 MALIGN (Johnson and Overington 1993). The coordinates for the NADP⁺ ligand were copied from
34 2XNJ[A] (Musumeci et al. 2011) to 3FPK[A] [Kim et al. to be published], which was then used as
35 template for modelling FNRL in complex with FAD and NADP⁺. All sequences except FNRL and
36 3FPK[A] were deleted from the alignment prior to modelling. The structural model for FNRL (Ser56
37 – Phe295) was generated with MODELLER (Sali and Blundell, 1993) and the model with the lowest
38 DOPE-score was chosen for further analysis. The model quality was assessed with PROCHECK
39 (Laskowski et al. 1993), ProSA-web (Sippl 1993, Wiederstein and Sippl 2007), ProQ (Wallner and
40 Elofsson 2003), and MODFOLD (Maghrabi et al. 2017, McGuffin et al. 2013), as well as by
41 superimposition with the template. PyMOL (Schrödinger LLC) and ESPript 3.0 (Gouet et al. 1999)
42 were used to generate pictures of the model and the alignments, respectively.
43
44
45
46
47
48
49
50
51
52
53
54
55
56
57
58
59
60

Overexpression and purification of proteins

The coding sequence of At1g15140 without the predicted transit peptide (first 47 amino acids) was PCR amplified from *A. thaliana* cDNA with the following primers: fw: 5'-TATACATATGGCCGCCGCGTTC and rev: 5'-TATAAAGCTTTCAAAAGTTTTTGAG. The PCR product was cloned into the vector pET-28a(+) (Novagen) using NdeI and HindIII restriction sites, which yielded a construct expressing N-terminally His6-tagged FNRL protein (268 aa, MW: 28.8. kDa). The recombinant protein was expressed in *E. coli* BL21(DE3). Cells were lysed (50 mM Na-phosphate – 300 mM NaCl pH 7.5 with freshly added 100 μ M FAD and EDTA-free Pierce Protease Inhibitor Tablet (Thermo Scientific)) in French Press (Constant Systems Ltd) using 20 kpsi pressure. The cell lysate was cleared by centrifugation (18000 rpm in Sorvall SS-34, 30 min at 4°C) and the supernatant mixed with an equal volume of equilibration buffer (50 mM Na-phosphate, 300 mM NaCl, 10 mM Imidazole pH 7.5). Proteins were loaded onto a 1.5 ml HisPur™ Cobalt Resin (Thermo Scientific) gravity flow column packed into 5 ml Pierce™ Disposable Column (Thermo Scientific). The column was washed with equilibration buffer and the protein eluted with 50 mM Na-phosphate, 300 mM NaCl, 150 mM Imidazole pH 7.5. The protein was filtered through a 0.2 μ m filter and further purified using an ÄKTA purifier UPC (GE Healthcare Life Sciences) equipped with a HiLoad 16/600 Superdex 200 PG column. Gel filtration was performed in 20 mM HEPES, 300 mM NaCl pH 7.5 with 0.15 ml min⁻¹ flow rate. AtFd1, ZmFNR2 and AtFdC1 were expressed and purified as described (Hanke et al. 2004, Okutani et al. 2005, Voss et al. 2011), respectively.

Spectroscopic assays

UV/Vis spectra were recorded on Lambda 25 UV/Vis spectrometer (PerkinElmer). The molar absorption coefficient for FNRL was determined in 10 mM HEPES, 150 mM NaCl, pH 7.5 (Macheroux 1999). Fluorescence spectra were carried out at 15° C on a Cary Eclipse (Varian) spectrofluorimeter: emission spectra in aromatic (300-500 nm) and FAD (500–800 nm) regions were obtained upon excitation at 280 nm and 460 nm, respectively. Circular dichroism (CD) spectra were obtained on a Chirascan spectropolarimeter (Applied Photophysics), at 15° C, using 0.1 cm or 1 cm pathlength cuvettes, for far-UV and near UV-visible, respectively. Mean residue molar ellipticity (Θ_{MRW} , degrees cm² dmol⁻¹) was calculated on the basis of 268 residues. Interaction with NADP⁺ was visualized by difference absorption spectroscopy upon titrating FNRL_{ox} (20 μ M) with NADP⁺ (0-64 μ M) in 50 mM HEPES, 300 mM NaCl, pH 7.0, 5% glycerol, at 15° C (Medina et al. 2001).

Steady-state kinetics measurements

Rates for cytochrome c (Cyt *c*) reduction by FNRL were determined at 550 nm in 10 mM HEPES – 150 mM NaCl pH 7.5 using 20 μ M Cyt *c* from equine heart (Sigma, BioUltra, >99% pur.), 100 μ M NADPH or NADH and 1.33 μ g FNRL. The diaphorase activity was measured at 600 nm using 50 mM HEPES at pH values of 6.8-8.2 and 50 mM TRIS at pH 7.1-8.6. In all cases ionic strength was set to 300 mM with NaCl. Reaction mixtures consisted of 100 nM FNRL, 40 μ M 2,6-

dichlorophenolindophenol (DCPIP) and 200 μM NADPH. Optimal salt concentration for maximal activity was determined by measuring DCPIP reduction in 50 mM HEPES pH 7.0 with variable salt concentrations (0-500 mM NaCl). Kinetic parameters for the FNRL diaphorase activity were determined using DCPIP ($\Delta\epsilon_{620\text{nm}}$ 21 $\text{mM}^{-1} \text{cm}^{-1}$) in 50 mM HEPES, 300 mM NaCl, pH 7.0, at 25°C (Medina et al., 2001). Reaction mixtures contained 50 nM FNRL, 100 μM DCPIP and 0-50 μM NADPH. K_m and k_{cat} values were obtained by fitting the dependence of the observed initial rates on the NADPH concentration to the Michaelis-Menten equation. Errors in K_m and k_{cat} were $\pm 20\%$ and $\pm 10\%$, respectively.

Stopped-flow pre-steady-state kinetic measurements

Reduction of FNRL_{ox} by NADPH was followed by evolution of the absorption spectra (400-800 nm) using a SX17.MV stopped-flow with a photodiode detector (App. Photo. Ltd.) (Peregrina et al. 2010, Tejero et al. 2007). After mixing, reaction samples contained 12 μM FNRL_{ox} and 12-200 μM NADPH. Reactions were carried out in 20 mM HEPES, 300 mM NaCl, pH 7.0, 5% glycerol, 10 mM glucose and 10 U ml^{-1} glucose oxidase (EC:1.1.3.4), at 10° C and under anaerobic conditions. Multiple wavelength data were processed using the X-Scan software (App. Photo. Ltd.). Time spectral deconvolution was performed using Pro-Kineticist v1.0.13 (App. Photo. Ltd.). Data were fitted to either two or three-step models, A→B→C or A→B→C→D, estimating observed conversion rate constants ($k_{A\rightarrow B}$, $k_{B\rightarrow C}$, $k_{C\rightarrow D}$) (Peregrina et al. 2010, Tejero et al. 2007). Errors in the determination of kinetic constants were $\pm 15\%$.

Thermal Shift Assays

Thermal shift assays (Forneris et al. 2009) were carried out on a Mx3005P real-time qPCR (Agilent Technologies) by following FAD release upon protein unfolding using 5 μM FNRL_{ox} in 50 mM HEPES, 300 mM NaCl, pH 7.0, 5% glycerol. The increase in FAD fluorescence was monitored using a FAM filter set ($\lambda_{\text{exc}} = 492 \text{ nm}$; $\lambda_{\text{em}} = 516 \text{ nm}$). Melting curves were registered from 25 to 100° C at 1° C min^{-1} . The midpoint denaturation temperature (T_m) was obtained by curve fitting to a sigmoidal equation. Thermal denaturation was also followed with increasing NADP⁺ concentrations (0-168 μM). The NADP⁺ dissociation constant, K_d , and the unfolding enthalpy of the protein in the absence of ligand, ΔH_0 , were determined by fitting the data to the equation (Cooper and McAuley-Hecht 1993)

$$\frac{\Delta T_m}{T_m} = \frac{nRT_m^0}{\Delta H_0} \ln \left(1 + \frac{[L]}{K_d} \right) \text{ Eq. 1}$$

where ΔT_m estimates the extent of the ligand-induced protein stabilization ($\Delta T_m = T_m - T_m^0$); with T_m^0 and T_m being the midpoint denaturation temperatures in the absence and the presence of ligand, respectively, and n the number of ligand binding sites considered here as unity.

Isothermal Titration Calorimetry (ITC)

ITC experiments were conducted using a high precision Auto-iTC200 system (MicroCal). Titrations were performed at 25° C in 50 mM HEPES, 300 mM NaCl, pH 7.0, 5% glycerol by injecting 2 μ L aliquots of 200 μ M NADP⁺ into the ITC cell containing 200 μ L of 80 μ M FNRL_{ox}. The binding enthalpy (ΔH), the association constant (K_a), and the stoichiometry of the binding were obtained through least-squares non-linear regression of the experimental data to a model for one binding site implemented in Origin 7.0 (*OriginLab*). The free energy change (ΔG) and the entropy change (ΔS) were obtained from basic thermodynamic relationships. The estimated error in the measured parameters is $\pm 15\%$ in K_a and K_d , $\pm 5\%$ in ΔG , and $\pm 10\%$ in ΔH and $-T\Delta S$.

Plant material, chloroplast isolation and protein extraction

A. thaliana (ecotype Col-0) was grown in 8 h light (100 μ mol m⁻² s⁻¹) /16 h darkness, 23 °C. For localization studies chloroplasts were isolated and fractionated as in (Lehtimäki et al. 2014). Soluble leaf proteins were extracted by grinding frozen rosettes in 5 mM sucrose, 10 mM HEPES-KOH pH 7.6, 5 mM MgCl₂, Pierce™ protease inhibitor (Thermo Scientific), filtered through Miracloth (Millipore) and centrifuged 10 min, 21 000 g at 4°C. Supernatant was collected as soluble protein fraction.

Gel electrophoresis and immunoblotting

Soluble *A. thaliana* proteins and protein samples from overexpression in *E. coli* were separated using 12% acrylamide gels with or without 6 M urea, as indicated. Gels were used for immunoblotting or they were stained with 0.1% Coomassie brilliant blue R-250 in 30% methanol, 5% acetic acid. Gels were blotted to Immobilon®-P PVDF (Merck Millipore) membrane, and immunolabeled with a custom made FNRL peptide antibody (against peptide CDGVSNDKLLKNF) (1:10 000) (Agrisera, Vännas, Sweden) or the D1 protein antibody (1:8000; Kettunen et al. 1996) followed by labelling with goat anti-rabbit-HRP antibody (1:50 000, Agrisera) and spraying with Advansta WesternBright ECL spray. Detection was performed with LI-COR C-Digit scanner using high sensitivity setting. Ferredoxin experiments were performed essentially as described previously (Okutani et al. 2005), but using *Arabidopsis* Fd1 and AtFdC1.

Quantitative RT-PCR

Total leaf RNA was isolated using Plant RNA Isolation Kit (Agilent Technologies, Santa Clara, CA, USA), cDNA synthesis and quantitative RT-PCR were performed as described (Rantala et al. 2016) using 5'-ACACGCCATCTCCGTTTATC-3' and 5'-GGAGCGTTTGAAATGTCGAT-3' as primers. At2g28390 and At4g34270 were used as reference genes (Hong et al. 2010). Data were analysed with QBASE PLUS software (Biogazelle NV, <http://www.biogazelle.com>).

Results

Bioinformatic analysis and structural modelling

Domain analysis of the FNRL primary sequence predicted an N-terminal Fd reductase-type FAD-binding domain (amino acids 56-162) and a C-terminal oxidoreductase FAD/NAD(P)-binding domain (amino acids 177-277), consistent with the tertiary structures used for the structure based sequence alignment. Furthermore, the typical sequence motifs for these domains (Dym & Eisenberg, 2001) are mostly conserved in FNRL (Fig. S1), except for the RxY(S/T) motif. Typically, this motif binds to the pyrophosphate of FAD, which indicates that the interactions between FAD and FNRL might be slightly different. FNRL resembles bacterial FPRs more than plastidic FNR since it lacks the amino acids directly after $\beta 5$ which normally form the plastidic FNR β -hairpin structure. This supports the choice of *Salmonella typhimurium* FPR (PDB accession code 3FPK; Kim et al., to be published) as a template for the structural modelling of FNRL and the modelled 3D fold, although the sequence identity between *Salmonella typhimurium* FPR and FNRL is low (Table S1). Moreover, quality control checks with multiple programs show that it is a good and reliable model (Table S2). It was experimentally determined that FAD is the FNRL cofactor (see below). Hence, FNRL likely folds into an FAD-binding N-terminal domain comprising a six-stranded β -sheet and one α -helix, as well as a C-terminal NADP⁺-binding α/β domain with a five-stranded β -sheet with a pair of α -helices on each side (Fig. 1A). The FAD-binding site in the predicted 3D model for FNRL is highly hydrophobic, with FAD bound in a bent conformation typically seen in bacterial FPRs (Fig. 1B). Hydrogen bonds from Ser and Thr residues contribute to the specificity and affinity, with Ser114 being especially important and conserved throughout the Fd-reductase superfamily. On the contrary, NADP⁺ is expected to bind through electrostatic interactions from positively charged Arg and Lys residues to the negatively charged phosphate groups, while several polar residues contribute with hydrogen bonds throughout the length of the molecule.

Spectroscopic properties of recombinant His6-FNRL

To study the biochemical properties of FNRL, we first expressed the His6-tagged protein in *E. coli* and purified it with average yield of 3.0 mg l⁻¹. In agreement with the molecular weight (28.8 kDa), SDS-PAGE indicated that the MW of purified FNRL was ca. 28 kDa (Fig. S2). Purified FNRL_{ox} exhibited a yellow colour (Fig. S2) and showed the typical absorption spectrum of a flavoprotein, with characteristic maxima at 269 nm, 380 nm (flavin band-II) and 460 nm (flavin band-I) (Fig. 2A). The purified protein showed $\text{Abs}_{269\text{nm}}/\text{Abs}_{461\text{nm}} = 6.71$. Thermal release of the cofactor identified it as FAD, and allowed determination of the extinction coefficient of FNRL_{ox} at 460 nm, giving the value of 11.4 mM⁻¹ min⁻¹. Fluorescence spectra of FNRL_{ox} (Fig. 2B and 2C) showed maxima at 332 nm and 525 nm, consistent with fluorescence of Trp residues in a folded protein and of the FAD cofactor. The relatively low intensity of the band at 525 nm suggests that the isoalloxazine ring is embedded within

1
2
3 the protein. The far-UV CD spectrum of the protein showed a negative band at 208 nm typical of a
4 secondary α -helix structure (Fig. 2D). The negative band around 222 nm, also typical of α -helix,
5 appeared like a shoulder, probably because of the content of β -sheet. The near-UV-Vis CD spectrum
6 showed a maximum at 260 nm and a sharp minimum at 296 nm, as well as two local minima at 390
7 and 490 nm related with the FAD cofactor signal (Fig. 2E).
8
9

10
11 *FNRL is reduced by NADPH and shows very weak interaction with AtFdI*

12 We first evaluated the ability of FNRL to transfer electrons from either NADPH or NADH to Cyt *c*.
13 NADPH yielded a reduction rate of $48.7 \mu\text{mol min}^{-1}\mu\text{mol}^{-1}$ enzyme while no activity was observed
14 with NADH (Fig. S3). Therefore, FNRL accepts two electrons from NADPH and is able to provide
15 then one at a time to Cyt *c*. Since Cyt *c* reduction is an artificial assay with significant background
16 activity, we then confirmed that FNRL had diaphorase activity and could also efficiently catalyse
17 NADPH dependent DCPIP reduction. The diaphorase assay was used to determine optimal reaction
18 conditions. Buffers with a range of pH values were chosen to represent the physiological pH range of
19 the stroma, and HEPES and TRIS buffers were tested. FNRL had higher activity in a neutral to
20 slightly acidic pH (Fig. 3A), but the overall effect was only 20 to 30% more compared to more basic
21 pH. In contrast, buffer salinity had a dramatic impact; maximal activity was obtained in a buffer
22 containing 300 mM NaCl (Fig. 3B); activity in these conditions was four times higher than without
23 added NaCl. We then evaluated the enzyme kinetic parameters using the DCPIP diaphorase assay.
24 The rate followed a saturation Michaelis-Menten profile over NADPH concentrations (Fig. 3C),
25 which allowed determination of; $k_{\text{cat}} = 3.24 \pm 0.17 \text{ s}^{-1}$, $K_{\text{m}}^{\text{NADPH}} = 1.6 \pm 0.3 \mu\text{M}$ and $k_{\text{cat}} / K_{\text{m}}^{\text{NADPH}} = 2.0$
26 $\pm 0.4 \mu\text{M}^{-1} \text{ s}^{-1}$.
27
28
29
30
31
32
33
34
35

36 We next used differential spectroscopy to evaluate whether NADP^+ binding perturbs the FAD
37 environment of FNRL_{ox} , observing the appearance of small differential absorption peaks at 387, 461
38 and 495 nm (Fig. 3D). This suggests that coenzyme binding somehow alters the FAD environment. In
39 plant FNRs peaks around 500 nm have been reported as indicative of flavin and nicotinamide ring
40 stacking (Medina et al. 2001). The magnitude of these peaks was relatively small, suggesting a low
41 percentage of occupation. We also used ITC to estimate binding parameters of NADP^+ to FNRL_{ox} .
42 Thermograms for the titration of FNRL_{ox} with NADP^+ confirmed binding (Fig. 3E), but the sample
43 became turbid during the assay. Indeed, data fitting indicated that a very small fraction (~8%) of
44 protein had bound coenzyme over the full course of the measurement, with apparent values for K_{d} , ΔH
45 and $-T \cdot \Delta\text{S}$ of $5.5 \pm 0.9 \mu\text{M}$, $-15.7 \pm 0.5 \text{ kcal mol}^{-1}$ and $8.53 \pm 0.5 \text{ kcal mol}^{-1}$, respectively. Low
46 occupancy results suggest that during difference spectroscopy and ITC titrations a significant fraction
47 of the protein is destabilized, in agreement with sample turbidity observed at the end of
48 experiments. Thermal denaturation of FNRL_{ox} produced the concomitant fluorescence increase of its
49 isoalloxazine ring, as a consequence of its greater exposure to the solvent. These data allow
50
51
52
53
54
55
56
57
58
59
60

determination of a T_m^0 of 38.6° C for the unfolding process (Fig. 3F). In the presence of $NADP^+$, a coenzyme concentration dependent shift (T_m) was observed (Figs. 3F and inset). Fitting of T_m to Eq. 1 (Fig. 3F inset) allowed us to determine a K_d value of $1.6 \pm 0.1 \mu M$ for the binding of one $NADP^+$ molecule to $FNRL_{ox}$, as well the $FNRL$ thermal denaturation enthalpy, which was $116 \pm 2 \text{ kcal mol}^{-1}$ (considering a 1:1 stoichiometry for $NADP^+$ binding). This ΔH value is in the range expected for a protein of this size, indicating that this method provides us with a robust K_d value based on 100% occupancy. Altogether, these data indicate that the affinity of $FNRL_{ox}$ for $NADP^+$ is in the low micromolar range.

The reduction of $FNRL_{ox}$ by $NADPH$ was also evaluated under pre-steady-state anaerobic conditions. Spectral evolution showed a slight decrease in absorption of the flavin band-I (462 nm) concomitant with the appearance of a long-wavelength absorbance band centred around 577 nm (Fig. 3G). This type of band is attributed to charge-transfer interactions between the oxidized flavin isoalloxazine ring and the nicotinamide ring of $NADPH$, FAD_{ox} - $NADPH$ charge-transfer complexes (CTC) (Batie and Kamin, 1986, Lans et al. 2010, Sánchez-Azqueta et al. 2014, Tejero et al. 2007). Evolution of absorption in both flavin band-I and CTC bands in the following spectra indicates flavin reduction by HT without the appearance of other CTC bands. Spectral evolution best fits to a two-step model at coenzyme:enzyme ratios below 5, while at higher coenzyme concentrations an additional slow process that completes flavin reduction is also observed (Figs. 3G and 3H). Transformation of species A into B relates to CTC formation ($k_{A \rightarrow B} = k_{obsCTC}$) (Fig. 3H). Transformation of species B into species C can be related to HT ($k_{B \rightarrow C} = k_{obsHT}$), but without producing full reduction of the protein. k_{obsCTC} and k_{obsHT} hardly increase with coenzyme concentrations, giving maximum values of $2.1 \pm 0.2 \text{ s}^{-1}$ and $1 \pm 0.1 \text{ s}^{-1}$ at the ratio of 5. These values are in the same range as k_{cat} , indicating that both processes are relevant for catalysis. Transformation of C into D is only observed at high $NADPH$ concentrations and with considerably slower $k_{C \rightarrow D}$ values. Therefore, this process does not appear relevant to catalysis, and might rather be an artefact related to the absence of an electron acceptor or to the binding of excess $NADPH$ to the reduced protein. Unfortunately, we were not able to similarly evaluate the ability of $FNRL_{red}$ to reduce $NADP^+$. Spectral changes of $FNRL_{ox}$ on photoreduction indicate flavin reduction, although the process resulted accompanied by a drift of the spectral baseline suggestive of turbidity (not shown).

Intriguingly, in contrast to FNR proteins, interaction of $FNRL$ with ferredoxin appears weak. Firstly, direct reduction of Cyt *c* by $FNRL$ in the presence of $NADPH$ occurs efficiently even in the absence of Fd (Fig. S3). Secondly, when Fd was immobilised on sepharose resin and challenged by loading the column with $FNRL$, $FNRL$ showed very weak interaction, and eluted at extremely low ionic strength, while the control $ZmFNR2$ (from *Zea mays*) bound strongly in a salt dependent manner (Fig. 3I), as expected from its high affinity for Fd (Okutani et al. 2005). As the *Arabidopsis* genome encodes several Fd -like proteins as well as Fds , we investigated whether one of these, $FdC1$, could be

1
2
3 the electron transfer partner, rather than classical photosynthetic Fd. We therefore repeated the resin
4 binding experiment using the Fd-like protein FdC1 (Voss et al. 2011), but FNRL did not show a
5 strong interaction with this electron carrier protein (Figure S4), indicating that this is not the case.
6
7

8 *Phylogenetic analysis and location of FNRL in planta*

9
10 Orthologues of the *AtFNRL* gene were found in all monocot (*Oryza sativa*, *Zea mays*) and dicot
11 (*Arabidopsis lyrata*, *Solanum lycopersicum*, *Populus trichocarpa*, *Brassica rapa*, *Capsella rubella*)
12 plant species studied, as well as in moss (*Physcomitrella patens*) and green alga (*Chlamydomonas*
13 *reinhardtii*), while no *FNRL* orthologue was identified in the cyanobacterium *Synechocystis* sp. PCC
14 6803 (Fig. S5). According to GreenCut2 classification, *FNRL* belongs into the PlastidCut group, and
15 orthologues are also found in a number of cyanobacterial species (Karpowicz et al. 2011), indicating
16 an important role in plastid metabolism. Moreover, immunoblotting of fractionated chloroplasts using
17 the *FNRL*-specific antibody (Fig. S6) showed that *FNRL* exists as a soluble protein in chloroplast
18 stroma (Fig. 4A). When the expression of *FNRL* gene during the day-night cycle was studied with
19 quantitative RT-PCR, it was evident that expression of the *FNRL* gene showed a clear diurnal
20 fluctuation, with highest expression in the middle of the light period and lowest expression in the
21 middle of the dark period (Fig. 4B). However, the amount of protein showed no fluctuation and
22 remained stable throughout the day (Fig. 4B).
23
24
25
26
27
28
29

30 **Discussion**

31
32 Chloroplasts contain a number of flavoproteins and flavoenzymes, the leaf-type FNR being the best
33 characterized member of this group. As the primary structure of *FNRL* shares marked similarities
34 with bacterial FPRs, structural and functional similarities might also be expected. Indeed, our
35 experimental results show that *FNRL* binds FAD (Fig. 2). In addition, sequence analysis and
36 structural modeling suggests that that *FNRL* folds into a similar structure as FPRs with both FAD and
37 NADP^+ binding to their predicted domains. The C-terminal Phe in *FNRL* is modeled to stack with the
38 flavin ring of FAD, since this position has a conserved aromatic residue in the studied FPRs and FNR
39 structures. However, we cannot rule out the possibility that the C-terminal Phe might instead stack
40 with the adenosine ring of FAD in a similar way to the final C-terminal residue (Trp) in the template.
41 Although *FNRL* catalyses oxidation of NADPH, FNRL_{ox} is considerably less efficient than plastid
42 FNRs (both leaf-type and root-type enzymes), mainly as consequence of its relatively low turnover
43 rate. Indeed, maize leaf-type FNR, maize root-type FNR and cyanobacterial FNR from *Anabaena*
44 show turnovers of 44 s^{-1} , 28 s^{-1} and 81.5 s^{-1} , respectively, in the same assay (Medina et al. 2001, Onda
45 et al. 2000). K_m^{NADPH} values are in the same range for the cyanobacterial and leaf type FNRs, while
46 higher affinities are found for the root enzymes. Regarding bacterial FPRs, enzymes from
47 *Xanthomonas anoxopodis citri* and *Rhodobacter capsulatus* also show larger k_{cat} values (122 s^{-1} and
48 20 s^{-1} respectively) than FNRL_{ox} , as well as K_m^{NADPH} values ($11 \text{ }\mu\text{M}$ and $85 \text{ }\mu\text{M}$ respectively)
49
50
51
52
53
54
55
56
57
58
59
60

1
2
3 (Bortolotti et al. 2014, Tondo et al. 2011). This latter fact results in the *R. capsulatus* enzyme being
4 even less efficient than FNRL.
5

6
7 Although FNRL resembles leaf-type FNR in favouring NADPH over NADH (Fig. S3), FNRL does
8 not appear to interact with the AtFd1 and AtFdC1 proteins (Fig. 3I and Fig. S4). This result is
9 supported by the sequence analysis, which implies that the known Fd-binding residues in plastidic
10 FNRs (Kurusu et al., 2001, Mulo and Medina, 2017) are markedly different from FNRL (Fig. S1).
11 These results are in line with the previous finding showing that inactivation of the two *A. thaliana*
12 leaf-type FNR isoforms is lethal (Lintala et al. 2012), further supporting the view that FNRL does not
13 have redundant function(s) with leaf-type FNRs. It remains to be seen whether principle function of
14 FNRL is as a diaphorase, oxidising NADPH and reducing a specific metabolite, or whether it has
15 protein electron transfer partners. The *A. thaliana* genome encodes genes for 6 [2Fe-2S] cluster Fd
16 type proteins. Three of these (AtFd1, AtFd2 and AtFd3) are standard leaf and root isoforms, capable
17 of supporting classical Fd-dependant reactions such as NADP⁺ photoreduction, nitrite and sulfur
18 assimilation (Hanke et al., 2004). If FNRL interacted with any of these, some degree of interaction
19 with the Fd1 column (Figure 3I) would be expected. It is possible that either Fd4 or one of the novel
20 [2Fe-2S] Fds with extended C-termini (FdC1 and FdC2) could act as electron transfer partners. Unlike
21 FNRL (Fig. S5), Fd4 has no known homologues in other plant species (Hanke et al., 2004), and
22 therefore seems an unrealistic candidate. FdC1 can accept electrons from PSI (Voss et al., 2011), and
23 we therefore checked whether this might be an electron transfer partner with FNRL, but also found
24 that interaction did not occur. FdC2 is highly unstable (unpublished data), and therefore not amenable
25 to the Fd-resin interaction assay. We therefore cannot discount it as a possible interaction partner.
26
27

28
29 FNRL is considerably slower in the HT process from NADPH than the leaf-type, root-type or
30 bacterial FNRs (Fig. 3; Bortolotti et al. 2014, Sánchez-Azqueta et al. 2012, 2014, Tejero et al. 2007).
31 Moreover, the reduction of FNRL by NADPH differs with respect to the stabilization of FNRL CTCs
32 (Bortolotti et al. 2014, Peregrina et al. 2010, Sánchez-Azqueta et al. 2012, 2014, Tejero et al. 2007).
33 Notably, differences in CTCs stabilization have also been reported between bacterial-type FPRs
34 relative to plastidic FNRs, as well as upon mutation of key residues in plastid FNRs (Bortolotti et al.
35 2014, Lans et al. 2010, Peregrina et al. 2010, Sánchez-Azqueta et al. 2014). Such differences are
36 related to dissimilarities in the geometric disposition of the reacting rings in the catalytically
37 competent complexes, in the nature of residues at the *re*-face of the isoalloxazine where the coenzyme
38 nicotinamide moiety is expected to stack for catalysis, or to the bipartite binding of the coenzyme
39 (Sánchez-Azqueta et al. 2014). These findings and the structural model of FNRL (Fig. 1) suggest that
40 the coenzyme approach and final geometry of the reacting complex of FNRL will be more similar to
41 that expected in bacterial FPRs than to plastidic-FNRs. Finally, the capacity of FNRL_{ox} to be fully
42 reduced by NADPH, combined with the fact that only a small percentage of FNRL molecules are in a
43
44
45
46
47
48
49
50
51
52
53
54
55
56
57
58
59
60

1
2
3 conformation able to interact with the oxidized form of the coenzyme, suggests that the *in vivo*
4 equilibrium of the FNRL reaction favours NADPH oxidation over the reverse process.
5

6 7 **Author contributions**

8
9 P.M., T.A.S., M.M., G.H., B.B., M.M.K., N.L. and K.M.D. designed the experiments and M.M.K.,
10 G.G. K.M.D., N.L., A.V-C., M.P. and M.N. performed research. P.M., T.A.S., M.M., M.M.K., and
11 K.M.D. analysed the data. P.M., M.M., T.A.S., K.M.D. and M.M.K. wrote the manuscript and all
12 authors revised and approved it.
13
14

15 16 **Acknowledgements**

17
18 This study was financially supported by Academy of Finland (307335 “Centre of Excellence in
19 Molecular Biology of Primary Producers”, Doctoral Programme in Molecular Life Sciences at the
20 University of Turku, the Spanish Ministry of Economy, Industry and Competitiveness (MINEICO)
21 (BIO2016-75183-P AEI/FEDER, UE to M.M.), the Government of Aragón-FEDER (B18), Åbo
22 Akademi Graduate School and Sigrid Jusélius Foundation. We also want to thank Professor Mark S.
23 Johnson (Structural Bioinformatics Laboratory, Åbo Akademi University) for the excellent computing
24 facilities. Use of Biocenter Finland infrastructure at Åbo Akademi (bioinformatics, structural biology
25 and translational activities is acknowledged. BB acknowledges support from the Cluster of integrated
26 protein science Munich, CIPSM.
27
28
29
30
31

32 33 **References**

- 34 Acheson JF, Moseson H, Fox BG (2015) Structure of T4moF, the toluene 4-monooxygenase
35 ferredoxin oxidoreductase. *Biochemistry* 54: 5980-8
36
37
38 Aliverti A, Pandini V, Pennati A, de Rosa M, Zanetti G (2008). Structural and functional diversity of
39 ferredoxin-NADP⁺ reductases. *Arch Biochem Biophys* 474: 283-291
40
41
42 Arnon DI (1991) Photosynthetic electron transport: Emergence of a concept, 1949-59. *Photosynth Res*
43 29: 117-131
44
45
46 Batie CJ and Kamin H (1984) Ferredoxin:NADP⁺ oxidoreductase. Equilibria in binary and ternary
47 complexes with NADP⁺ and ferredoxin. *J Biol Chem* 259: 8832-8839
48
49
50 Bortolotti A, Sánchez-Azqueta A, Maya CM, Velázquez-Campoy A, Hermoso JA, Medina M, Cortez
51 N (2014) The C-terminal extension of bacterial flavodoxin-reductases: involvement in the hydride
52 transfer mechanism from the coenzyme. *Biochim Biophys Acta* 1837: 33-43
53
54
55 Ceccarelli EA, Arakaki AK, Cortez N, Carrillo N (2004) Functional plasticity and catalytic efficiency
56 in plant and bacterial ferredoxin-NADP(H) reductases. *Biochim Biophys Acta* 1698: 155-165
57
58
59
60

1
2
3 Conrad KS, Manahan CC, Crane BR (2014) Phytochemistry of flavoprotein light sensors. *Nat Chem*
4 *Biol* 10: 801-809

5
6
7 Cooper A, McAuley-Hecht KE (1993) Microcalorimetry and the molecular recognition of peptides
8 and proteins. *Phil Trans R Soc Lond A* 345: 23-35

9
10
11 de Castro E, Sigrist CJ, Gattiker A, Bulliard V, Langendijk-Genevaux PS, Gasteiger E, Bairoch A,
12 Hulo N (2006) ScanProsite: Detection of PROSITE signature matches and ProRule-associated
13 functional and structural residues in proteins. *Nucleic Acids Res* 34 (Web Server issue): W362-5

14
15
16 Deng Z, Aliverti A, Zanetti G, Arakaki AK, Ottado J, Orellano EG, Calcaterra NB, Ceccarelli EA,
17 Carrillo N, Karplus PA (1999) A productive NADP⁺ binding mode of ferredoxin-NADP⁺ reductase
18 revealed by protein engineering and crystallographic studies. *Nat Struct Biol* 6: 847-853

19
20
21 Dym O, Eisenberg D (2001) Sequence-structure analysis of FAD-containing proteins. *Protein Sci* 10:
22 1712-28

23
24
25 Finn RD, Attwood TK, Babbitt PC, Bateman A, Bork P, Bridge AJ, Chang HY, Dosztányi Z, El-
26 Gebali S, Fraser M, Gough J, Haft D, Holliday GL, Huang H, Huang X, Letunic I, Lopez R, Lu S,
27 Marchler-Bauer A, Mi H, Mistry J, Natale DA, Necci M, Nuka G, Orengo CA, Park Y, Pesseat S,
28 Piovesan D, Potter SC, Rawlings ND, Redaschi N, Richardson L, Rivoire C, Sangrador-Vegas A,
29 Sigrist C, Sillitoe I, Smithers B, Squizzato S, Sutton G, Thanki N, Thomas PD, Tosatto SCE, Wu CH,
30 Xenarios I, Yeh LS, Young SY, Mitchell AL (2017) InterPro in 2017 — beyond protein family and
31 domain annotations. *Nucleic Acids Res* 45(Database issue): D190-D199

32
33
34 Forneris F, Orru R, Bonivento D, Chiarelli LR, Mattevi A (2009) ThermoFAD, a ThermoFluor-
35 adapted flavin ad hoc detection system for protein folding and ligand binding. *FEBS J* 276: 2833-
36 2840

37
38
39 Gouet P, Courcelle E, Stuart DI, Metz F (1999) ESPript: Analysis of multiple sequence alignments
40 in PostScript. *Bioinformatics* 15: 305-308

41
42
43 Hanke GT, Kimata-Arigo Y, Taniguchi I and Hase T (2004) A post genomic characterization of
44 *Arabidopsis* ferredoxins. *Plant Physiol* 134: 255–264

45
46
47 Hanke GT, Okutani S, Satomi Y, Takao T, Suzuki A, Hase T (2005) Multiple iso-proteins of FNR in
48 *Arabidopsis*: evidence for different contributions to chloroplast function and nitrogen assimilation.
49 *Plant Cell Environ* 28: 1146–1157

50
51
52 Hong SM, Bahn SC, Lyu A, Jung HS, Ahn JH (2010) Identification and testing of superior reference
53 genes for a starting pool of transcript normalization in *Arabidopsis*. *Plant Cell Physiol* 51: 1694-1706

1
2
3 Ingelman M, Ramaswamy S, Nivière V, Fontecave M, Eklund H (1999) Crystal structure of
4 NAD(P)H:flavin oxidoreductase from *Escherichia coli*. *Biochemistry* 38: 7040-9
5

6
7 Jelesarov I, De Pascalis AR, Koppenol WH, Hirasawa M, Knaff DB, Bosshard HR (1993) Ferredoxin
8 binding site on ferredoxin: NADP⁺ reductase. Differential chemical modification of free and
9 ferredoxin-bound enzyme. *Eur J Biochem* 216: 57-66
10

11
12 Johnson MS, Lehtonen JV (2000) Comparison of protein threedimensional structures. In D. Higgins,
13 & W. Taylor (Eds.), *Bioinformatics: Sequence, structure and databanks*. (pp. 15). Oxford, UK:
14 Oxford University Press
15

16
17 Johnson MS, Overington JP (1993) A structural basis for sequence comparisons: an evaluation of
18 scoring methodologies. *J Mol Biol* 233: 716-738
19

20
21 Jones DT (1999) Protein secondary structure prediction based on position specific scoring matrices. *J*
22 *Mol Biol* 292: 195-202
23

24
25 Jones P, Binns D, Chang HY, Fraser M, Li W, McAnulla C, McWilliam H, Maslen J, Mitchell A,
26 Nuka G, Pesseat S, Quinn AF, Sangrador-Vegas A, Scheremetjew M, Yong SY, Lopez R, Hunter S
27 (2014) InterProScan 5: genome-scale protein function classification. *Bioinformatics* 30: 1236-40
28

29
30 Karpowicz SJ, Prochnik SE, Grossman AR, Merchant SS (2011) The GreenCut2 resource, a
31 phylogenomically derived inventory of proteins specific to the plant lineage. *J Biol Chem* 286: 21427-
32 21439
33

34
35 Karplus PA, Daniels MJ, Herriott JR (1991) Atomic structure of ferredoxin-NADP⁺ reductase:
36 prototype for a structurally novel flavoenzyme family. *Science* 251: 60-66
37

38
39 Kettunen R, Tyystjärvi E, Aro E-M (1996) Degradation pattern of photosystem II reaction center
40 protein D1 in intact leaves: The major photoinhibition-induced cleavage site in D1 polypeptide is
41 located amino terminally of the DE loop. *Plant Physiol* 111: 1183-1190
42

43
44 Kim Y, Gu M, Stam J, Anderson WF, Joachimiak A, Center for Structural Genomics of Infectious
45 Diseases (To be published) Crystal Structure of Ferredoxin-NADP Reductase from *Salmonella*
46 *typhimurium*.
47

48
49 Kim Y, Mulligan R, Moy S, Joachimiak A, Midwest Center for Structural Genomics (To be
50 published) Crystal Structure of the Domain Comprising the Regions Binding NAD and FAD from the
51 NADH:Ubiquinone Oxidoreductase, Na Translocating, F Subunit from *Porphyromonas gingivalis*.
52
53
54
55
56
57
58
59
60

1
2
3 Kurisu G, Kusunoki M, Katoh E, Yamazaki T, Teshima K, Onda Y, Kimata-Arigo Y, Hase T (2001)
4 Structure of the electron transfer complex between ferredoxin and ferredoxin-NADP(+) reductase.
5 Nat Struct Biol 8: 117-21
6

7
8 Lans I, Peregrina JR, Medina M, García-Viloca M, González-Lafont A, Lluch JM (2010) Mechanism
9 of the hydride transfer between Anabaena Tyr303Ser FNR_{rd}/FNR_{ox} and NADP⁺/H. A combined pre-
10 steady-state kinetic/ensemble-averaged transition-state theory with multidimensional tunneling study.
11 J Phys Chem B 114: 3368-3379
12
13

14
15 Laskowski RA, Moss DS, Thornton JM (1993) Main-chain bond lengths and bond angles in protein
16 structures. J Mol Biol 231: 1049-1067
17

18
19 Lehtimäki N, Koskela MM, Dahlström KM, Pakula E, Lintala M, Scholz M, Hippler M, Hanke GT,
20 Rokka A, Battchikova N, Salminen TA, Mulo P (2014) Posttranslational modifications of
21 FERREDOXIN-NADP⁺ OXIDOREDUCTASE in Arabidopsis chloroplasts. Plant Physiol 166: 1764-
22 1776
23
24

25
26 Lehtonen JV, Still DJ, Rantanen VV, Ekholm J, Bjorklund D, Iftikhar Z, Huhtala M, Repo S, Jussila
27 A, Jaakkola J, Pentikäinen O, Nyrönen T, Salminen T, Gyllenberg M, Johnson MS (2004) BODIL: A
28 molecular modelling environment for structure-function analysis and drug design. J Comput Aided
29 Mol Des 18: 401-419
30
31

32
33 Letunic I, Doerks T, Bork P (2015) SMART: Recent updates, new developments and status in 2015.
34 Nucleic Acids Res 43(Database issue): D257-60
35

36
37 Lintala M, Allahverdiyeva Y, Kidron H, Piippo M, Battchikova N, Suorsa M, Rintamäki E, Salminen,
38 T, Aro E-M, Mulo P (2007) Structural and functional characterization of ferredoxin-NADP⁺-
39 oxidoreductase using knock-out mutants of *Arabidopsis*. Plant J 49: 1041-1052
40

41
42 Lintala M, Allahverdiyeva Y, Lehtimäki N, Kangasjärvi S, Keränen M, Rintamäki E, Aro E-M, Mulo
43 P (2009) Comparative analysis of leaf-type ferredoxin-NADP⁺-oxidoreductase isoforms in
44 *Arabidopsis thaliana*. Plant J 57: 1103-1115
45
46

47
48 Lintala M, Lehtimäki N, Benz P, Jungfer A, Soll J, Aro E-M, Bölder B, Mulo P (2012) Depletion of
49 leaf-type ferredoxin-NADP⁺-oxidoreductase results in permanent induction of photoprotective
50 mechanisms in chloroplasts of *Arabidopsis thaliana*. Plant J 70: 809-17
51
52

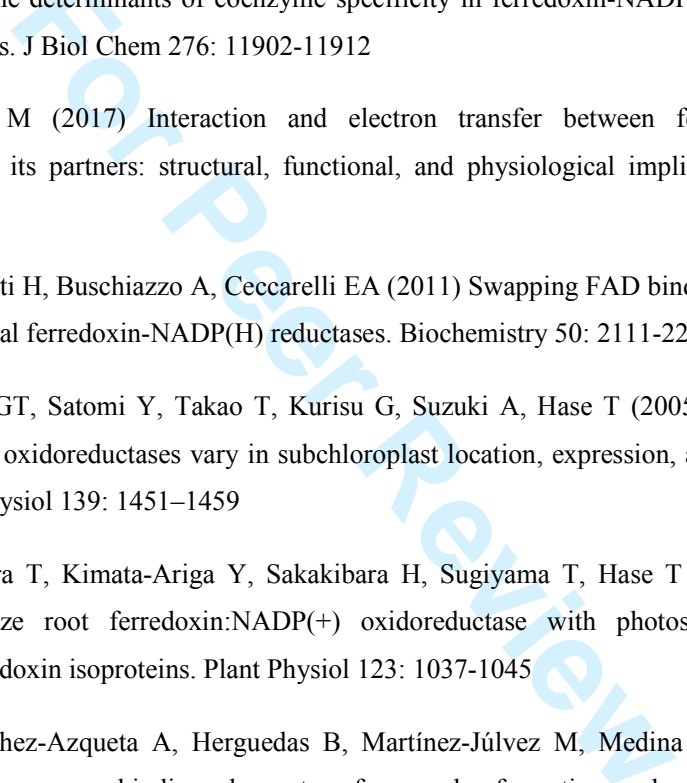
53
54 Macheroux P (1999) UV-visible spectroscopy as a tool to study flavoproteins. In: Chapman SK, Reid
55 GA (eds) Methods Mol Biol: Flavoprotein Protocols 131, Humana Press Totowa, New Jersey, pp 1-7
56
57
58
59
60

1
2
3 Maghrabi AHA, McGuffin LJ (2017) ModFOLD6: an accurate web server for the global and local
4 quality estimation of 3D protein models. *Nucleic Acids Res Epub ahead of print* doi:
5 10.1093/nar/gkx332
6

7
8 McGuffin LJ, Bryson K, Jones DT (2000) The PSIPRED protein structure prediction server.
9 *Bioinformatics* 16: 404-405
10

11
12 McGuffin LJ, Buenavista, MT, Roche DB (2013) The ModFOLD4 server for the quality assessment
13 of 3D protein models. *Nucleic Acids Res* 41(Web Server issue): W368-72
14

15
16 Medina M, Luquita A, Tejero J, Hermoso J, Mayoral T, Sanz-Aparicio J, Grever K, Gómez-Moreno
17 C (2001) Probing the determinants of coenzyme specificity in ferredoxin-NADP⁺ reductase by site-
18 directed mutagenesis. *J Biol Chem* 276: 11902-11912
19

20
21 Mulo P, Medina M (2017) Interaction and electron transfer between ferredoxin-NADP(+) 
22 oxidoreductase and its partners: structural, functional, and physiological implications. *Photosynth*
23 *Res*, in press
24
25

26
27 Musumeci MA, Botti H, Buschiazzo A, Ceccarelli EA (2011) Swapping FAD binding motifs between
28 plastidic and bacterial ferredoxin-NADP(H) reductases. *Biochemistry* 50: 2111-22
29

30
31 Okutani S, Hanke GT, Satomi Y, Takao T, Kurisu G, Suzuki A, Hase T (2005) Three maize leaf
32 ferredoxin:NADPH oxidoreductases vary in subchloroplast location, expression, and interaction with
33 ferredoxin. *Plant Physiol* 139: 1451-1459
34

35
36 Onda Y, Matsumura T, Kimata-Arigo Y, Sakakibara H, Sugiyama T, Hase T (2000) Differential
37 interaction of maize root ferredoxin:NADP(+) oxidoreductase with photosynthetic and non-
38 photosynthetic ferredoxin isoproteins. *Plant Physiol* 123: 1037-1045
39

40
41 Peregrina JR, Sánchez-Azqueta A, Herguedas B, Martínez-Júlvez M, Medina M (2010) Role of
42 specific residues in coenzyme binding, charge-transfer complex formation, and catalysis in *Anabaena*
43 ferredoxin-NADP⁺ reductase. *Biochim Biophys Acta* 1797: 1638-1646
44
45

46
47 Rantala M, Lehtimäki N, Aro EM, Suorsa M. 2016. Downregulation of TAP38/PPH1 enables LHCII
48 hyperphosphorylation in *Arabidopsis* mutant lacking LHCII docking site in PSI. *FEBS Lett.* 590: 787-
49 794
50

51
52 Sali A, Blundell TL (1993) Comparative protein modelling by satisfaction of spatial restraints. *J Mol*
53 *Biol* 234: 779-815
54
55

1
2
3 Sánchez-Azqueta A, Catalano-Dupuy DL, López-Rivero A, Tondo ML, Orellano EG, Ceccarelli EA,
4 Medina M (2014) Dynamics of the active site architecture in plant-type Ferredoxin-NADP(+)
5 reductases catalytic complexes. *Biochim Biophys Acta* 1837: 1730-1738
6
7

8 Sánchez-Azqueta A, Musumeci MA, Martínez-Júlvez M, Ceccarelli EA, Medina M (2012) Structural
9 backgrounds for the formation of a catalytically competent complex with NADP(H) during hydride
10 transfer in ferredoxin-NADP⁺ reductases. *Biochim Biophys Acta* 1817: 1063-1071
11
12

13 Schultz J, Milpetz F, Bork P, Ponting CP (1998) SMART, a simple modular architecture research
14 tool: Identification of signaling domains. *Proc Natl Acad Sci USA* 95: 5857-5864
15
16

17 Serre L, Vellieux FM, Medina M, Gómez-Moreno C, Fontecilla-Camps JC, Frey M (1996) X-ray
18 structure of the ferredoxin:NADP⁺ reductase from the cyanobacterium *Anabaena* PCC 7119 at 1.8 Å
19 resolution, and crystallographic studies of NADP⁺ binding at 2.25 Å resolution. *J Mol Biol* 263: 20-39
20
21

22 Sippl MJ (1993) Recognition of errors in three-dimensional structures of proteins. *Proteins* 17: 355-
23 362
24
25

26 Tejero J, Peregrina JR, Martínez-Júlvez M, Gutiérrez A, Gómez-Moreno C, Scrutton NS and Medina
27 M (2007) Catalytic mechanism of hydride transfer between NADP⁺/H and ferredoxin-NADP⁺
28 reductase from *Anabaena* PCC 7119. *Arch Biochem Biophys* 459: 79-90
29
30

31 Tondo ML, Musumeci MA, Delprato ML, Ceccarelli EA, Orellano EG (2011) Structural-functional
32 characterization and physiological significance of ferredoxin-NADP⁺ reductase from *Xanthomonas*
33 *axonopodis* pv. *citri*. *PLoS One* 6: e27124
34
35

36 Voss I, Goss T, Murozuka E, Altmann B, McLean KJ, Rigby SEJ, Munro AW, Scheibe R, Hase T,
37 Hanke GT (2011) FdC1, a novel ferredoxin protein capable of alternative electron partitioning,
38 increases in conditions of acceptor limitation at Photosystem I. *J Biol Chem* 286: 50–59
39
40

41 Wallner B, Elofsson A (2003) Can correct protein models be identified? *Protein Sci* 12: 1073-1086
42
43

44 Wiederstein M, Sippl MJ (2007) ProSA-web: Interactive web service for the recognition of errors in
45 three-dimensional structures of proteins. *Nucleic Acids Res* 35(Web Server issue): W407-10
46
47

48 49 50 51 **Supporting Information**

52 Additional Supporting Information may be found in the online version of this article:

53 Appendix Figure S1. Structure-based alignment of crystal structures homologous to FNRL aligned
54 with the sequence of FNRL and *A. thaliana*, maize and pea FNRs.
55
56

57 Appendix Figure S2. Purification of recombinant FNRL.
58
59
60

Appendix Figure S3. Reduction of cytochrome *c* by NADPH or NADH mediated by FNRL.

Appendix Figure S4. Affinity of AtFdC1 to FNRL.

Appendix Figure S5. Phylogenetic analysis of *Arabidopsis thaliana* FNRL.

Appendix Figure S6. Specificity of the FNRL antibody.

Appendix Table S1. Sequence identity table for FNRL and sequences in the alignment.

Appendix Table S2. Quality check results for the FNRL model.

Figure legends

Figure 1. Overall fold of the predicted 3D structure for FNRL and ligand binding site. (A) FNRL is likely to fold into a structure that resembles bacterial FPRs with an N-terminal ferredoxin reductase-type FAD-binding domain with six β -strands (green) and an α -helix (violet), as well as a C-terminal oxidoreductase FAD/NAD(P)-binding domain built from a central five-stranded β -sheet (green) and flanked by two α -helices on each side (pink). FAD and NADP⁺ are shown as sticks in grey. FNRL is more like bacterial FPRs than plastidic FNRs because of the lack of a β -hairpin structure typical for plastidic FNRs after β 5. For comparison, the magnification shows this area in FNRL (green) when superimposed on pea FNR (grey, β -hairpin in pink). (B) FAD likely binds to FNRL in a bent conformation typical for bacterial FPRs. The FAD-binding site is highly hydrophobic, while hydrogen bonds from Ser and Thr residues contribute to the specificity and affinity. Instead, NADP⁺ is bound through electrostatic interactions from positively charged Arg and Lys residues to the negatively charged phosphate groups, while several hydrogen bonds are formed from polar residues to the rest of the molecule.

Figure 2. Spectral properties of FNRL. (A) Visible absorption spectrum of FNRL (solid line) and of its released FAD cofactor (dotted line). (B) Fluorescence spectrum of FNRL (4.75 μ M) in the aromatics emission region recorded in 5 mM HEPES, 30 mM NaCl, pH 7.0. (C) Fluorescence spectrum of FNRL (47.5 μ M) in the flavin cofactor emission region recorded in 50 mM HEPES, 300 mM NaCl, pH 7.0. (D) Far-UV CD spectrum of FNRL (4.75 μ M) recorded in 5 mM HEPES, 30 mM NaCl, pH 7.0. (E) Near-UV-Vis CD spectrum of FNRL (4.75 μ M) recorded in 50 mM HEPES, 300 mM NaCl, pH 7.0. Fluorescence and CD spectra were recorded at 15° C.

Figure 3. FNRL activity with NADPH and interaction with NADP⁺. (A) The pH optimum was determined by measuring DCPIP reduction activity in buffers with different pH and constant ionic strength of 300 mM. (B) The salt optimum was determined by measuring DCPIP reduction activity in

1
2
3 buffers with variable NaCl concentration, but a constant pH of 7. (C) Michaelis-Menten profile for the
4 NADPH diaphorase activity of FNRL in 50 mM HEPES, 300 mM NaCl, pH 7.0, at 25° C. (n=3, ±
5 SD). (D) Difference absorption spectra elicited by the titration of FNRL_{ox} (20 μM) with NADP⁺ (0-70
6 μM) in 50 mM HEPES, 300 mM NaCl, pH 7.0, 5% glycerol at 25° C. (E) Experimental calorimetric
7 titration of 28 μM FNRL with NADP⁺ (200 μM in the ITC syringe). The upper and lower panels
8 show respectively the thermogram and the corresponding binding isotherms with integrated heats.
9 Experiments were carried out in 50 mM HEPES, 300 mM NaCl, 5% glycerol, pH 7.0 at 25° C. (F) T_m
10 shifts observed by differential scanning fluorescence upon increasing the NADP⁺ concentration (from
11 0 μM (black circles and thick black line) to 175 μM (light grey circles and thin light grey line) of a
12 sample containing 5 μM FNRL. Experiments were carried out in 50 mM HEPES, 300 mM NaCl, pH
13 7.0, 5% glycerol. Thermal stability curves are plotted against the normalized fluorescence signal. The
14 inset shows the dependence of $\Delta T_m/T_m$ on the NADP⁺ concentration and data fit to Eq. 1. (G) Spectra
15 recorded at 0.0002 s (thick black line), 0.15 s, 0.5 s, 1 s, 2 s, 4 s, 8 s, and 20 s (light grey line) after
16 mixing in the stopped-flow instrument of 24 μM FNRL_{ox} with 300 μM NADPH under anaerobic
17 conditions. The insert shows time evolution of the absorption at 460 nm (line, left y-axis) and 577 nm
18 (dotted line, right y-axis). Residuals for fittings are shown at the bottom. Experiments carried out in 20
19 mM HEPES, 300 mM NaCl, pH 7.0, 5% glycerol, 10 mM glucose, 10 U ml⁻¹ glucose oxidase, at 10°
20 C and under anaerobic conditions. (H) Absorbance spectra for the A (black), B (dark grey), C (grey)
21 and D (light grey) spectroscopic intermediate species obtained by global analysis. The insert shows
22 time evolution of spectroscopic species. (I) Affinity of AtFd1 to FNRL and ZmFNR2. Fd1 was
23 immobilized on sepharose and challenged by the addition of FNRL (bold line) or ZmFNR2 (line) in
24 50 mM Tris-HCl, pH 7.5 and 0 mM NaCl. Thereafter, a salt gradient in the same buffer to 300 mM
25 NaCl was applied to disrupt salt-bridging (gradients denoted by dashed-dotted and dotted lines
26 respectively) and elution of the protein followed at AU²⁸⁰.

27
28
29
30
31
32
33
34
35
36
37
38
39
40
41 **Figure 4.** Expression and location of FNRL. (A) A representative Western blot showing the
42 localization of FNRL. The proteins were separated using 12% SDS-PAGE with 6 M urea. D1 protein
43 was used as a thylakoid marker. (B) *FNRL* gene and FNRL protein expression during day-night
44 cycle. *FNRL* expression was studied with qRT-PCR (light grey) and protein amount with
45 immunoblotting (dark grey). Black bar on the x-axis depicts the dark period of the day and white bar
46 the light period.
47
48
49
50
51
52
53
54
55
56
57
58
59
60

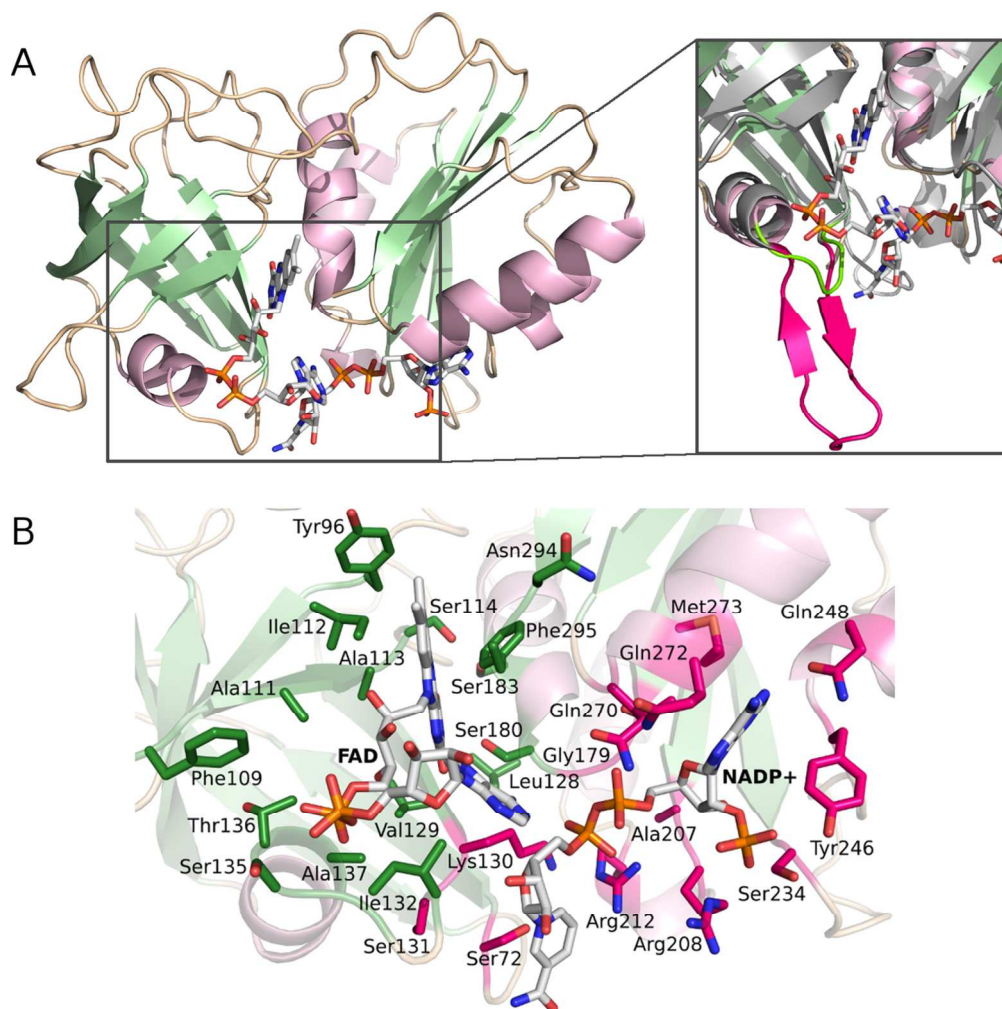


Figure 1. Overall fold of the predicted 3D structure for FNRL and ligand binding site. (A) FNRL is likely to fold into a structure that resembles bacterial FPRs with an N-terminal ferredoxin reductase-type FAD-binding domain with six β -strands (green) and an α -helix (violet), as well as a C-terminal oxidoreductase FAD/NAD(P)-binding domain built from a central five-stranded β -sheet (green) and flanked by two α -helices on each side (pink). FAD and NADP⁺ are shown as sticks in grey. FNRL is more like bacterial FPRs than plastidic FNRs because of the lack of a β -hairpin structure typical for plastidic FNRs after β 5. For comparison, the magnification shows this area in FNRL (green) when superimposed on pea FNR (grey, β -hairpin in pink). (B) FAD likely binds to FNRL in a bent conformation typical for bacterial FPRs. The FAD-binding site is highly hydrophobic, while hydrogen bonds from Ser and Thr residues contribute to the specificity and affinity. Instead, NADP⁺ is bound through electrostatic interactions from positively charged Arg and Lys residues to the negatively charged phosphate groups, while several hydrogen bonds are formed from polar residues to the rest of the molecule.

166x166mm (300 x 300 DPI)

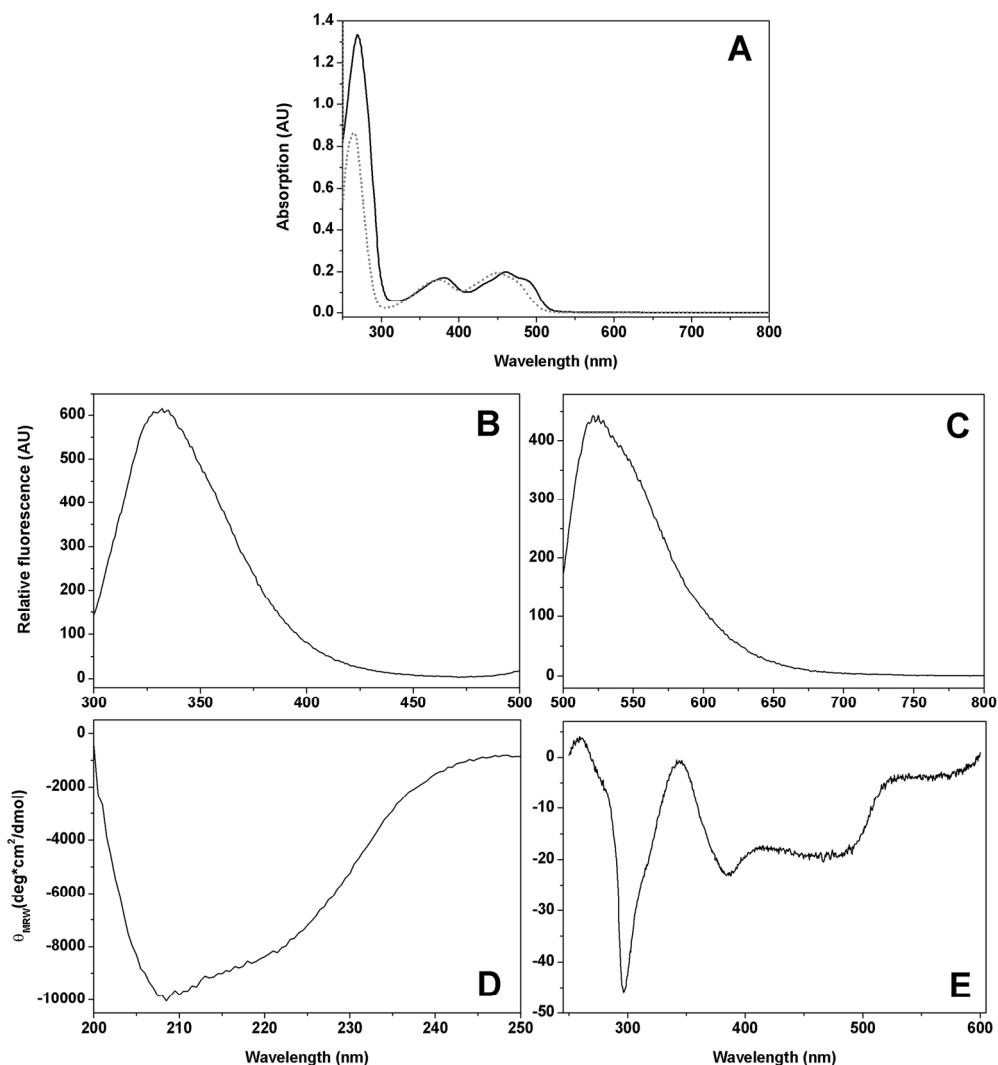


Figure 2. Spectral properties of FNRL. (A) Visible absorption spectrum of FNRL (solid line) and of its released FAD cofactor (dotted line). (B) Fluorescence spectrum of FNRL (4.75 μM) in the aromatics emission region recorded in 5 mM HEPES, 30 mM NaCl, pH 7.0. (C) Fluorescence spectrum of FNRL (47.5 μM) in the flavin cofactor emission region recorded in 50 mM HEPES, 300 mM NaCl, pH 7.0. (D) Far-UV CD spectrum of FNRL (4.75 μM) recorded in 5 mM HEPES, 30 mM NaCl, pH 7.0. (E) Near-UV-Vis CD spectrum of FNRL (4.75 μM) recorded in 50 mM HEPES, 300 mM NaCl, pH 7.0. Fluorescence and CD spectra were recorded at 15° C.

180x197mm (300 x 300 DPI)

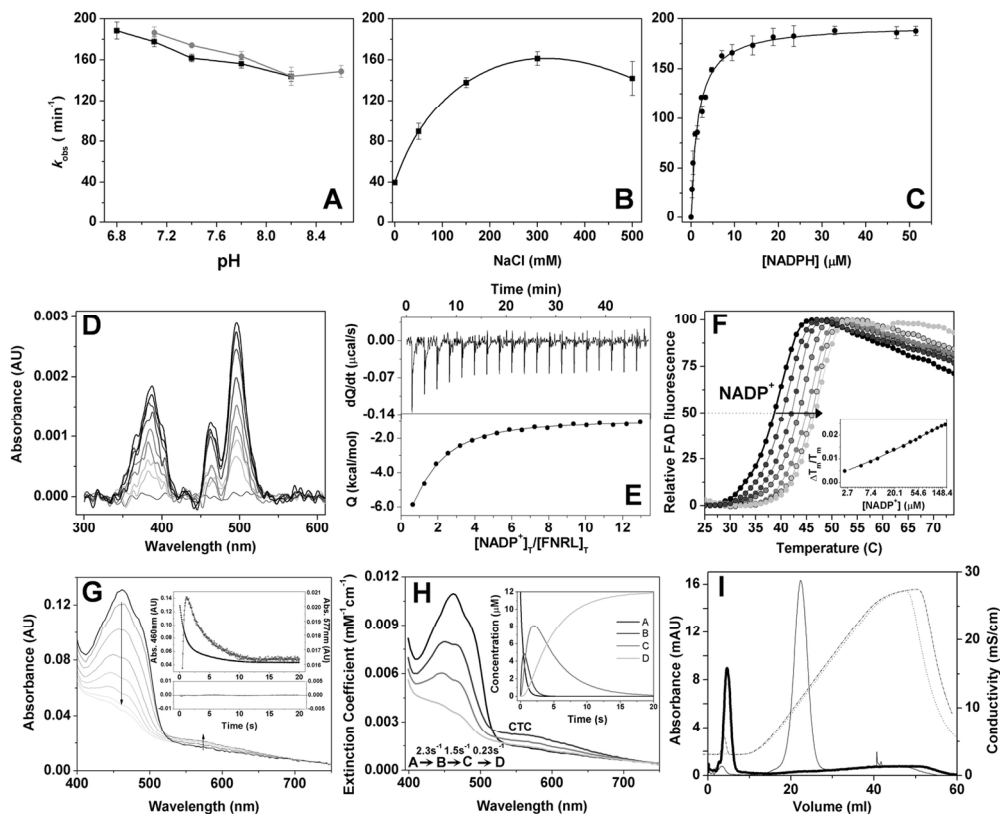
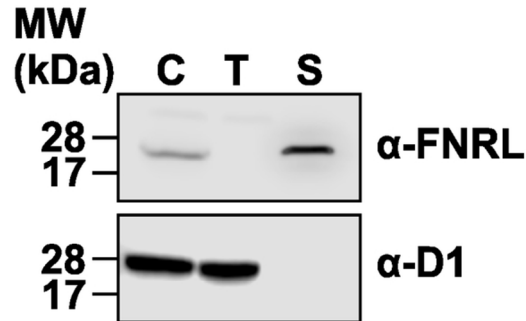


Figure 3. FNRL activity with NADPH and interaction with NADP⁺. (A) The pH optimum was determined by measuring DCPIP reduction activity in buffers with different pH and constant ionic strength of 300 mM. (B) The salt optimum was determined by measuring DCPIP reduction activity in buffers with variable NaCl concentration, but a constant pH of 7. (C) Michaelis-Menten profile for the NADPH diaphorase activity of FNRL in 50 mM HEPES, 300 mM NaCl, pH 7.0, at 25° C. ($n=3$, \pm SD). (D) Difference absorption spectra elicited by the titration of FNRL_{ox} (20 μ M) with NADP⁺ (0–70 μ M) in 50 mM HEPES, 300 mM NaCl, pH 7.0, 5% glycerol at 25° C. (E) Experimental calorimetric titration of 28 μ M FNRL with NADP⁺ (200 μ M in the ITC syringe). The upper and lower panels show respectively the thermogram and the corresponding binding isotherms with integrated heats. Experiments were carried out in 50 mM HEPES, 300 mM NaCl, 5% glycerol, pH 7.0 at 25° C. (F) T_m shifts observed by differential scanning fluorescence upon increasing the NADP⁺ concentration (from 0 μ M (black circles and thick black line) to 175 μ M (light grey circles and thin light grey line) of a sample containing 5 μ M FNRL. Experiments were carried out in 50 mM HEPES, 300 mM NaCl, pH 7.0, 5% glycerol. Thermal stability curves are plotted against the normalized fluorescence signal. The inset shows the dependence of $\Delta T_m/T_m$ on the NADP⁺ concentration and data fit to Eq. 1. (G) Spectra recorded at 0.0002 s (thick black line), 0.15 s, 0.5 s, 1 s, 2 s, 4 s, 8 s, and 20 s (light grey line) after mixing in the stopped-flow instrument of 24 μ M FNRL_{ox} with 300 μ M NADPH under anaerobic conditions. The insert shows time evolution of the absorption at 460 nm (line, left y-axis) and 577 nm (dotted line, right y-axis). Residuals for fittings are shown at the bottom. Experiments carried out in 20 mM HEPES, 300 mM NaCl, pH 7.0, 5% glycerol, 10 mM glucose, 10 U ml⁻¹ glucose oxidase, at 10° C and under anaerobic conditions. (H) Absorbance spectra for the A (black), B (dark grey), C (grey) and D (light grey) spectroscopic intermediate species obtained by global analysis. The insert shows time evolution of spectroscopic species. (I) Affinity of AtFd1 to FNRL and ZmFNR2. Fd1 was immobilized on sepharose and challenged by the addition of FNRL (bold line) or ZmFNR2 (line) in 50 mM Tris-HCl, pH 7.5 and 0 mM NaCl. Thereafter, a salt gradient in the same buffer to 300 mM NaCl was applied to disrupt salt-bridging (gradients denoted by dashed-dotted and dotted lines respectively) and elution of the protein followed at AU²⁸⁰.

1
2
3
4
5
6
7
8
9
10
11
12
13
14
15
16
17
18
19
20
21
22
23
24
25
26
27
28
29
30
31
32
33
34
35
36
37
38
39
40
41
42
43
44
45
46
47
48
49
50
51
52
53
54
55
56
57
58
59
60

For Peer Review

A



B

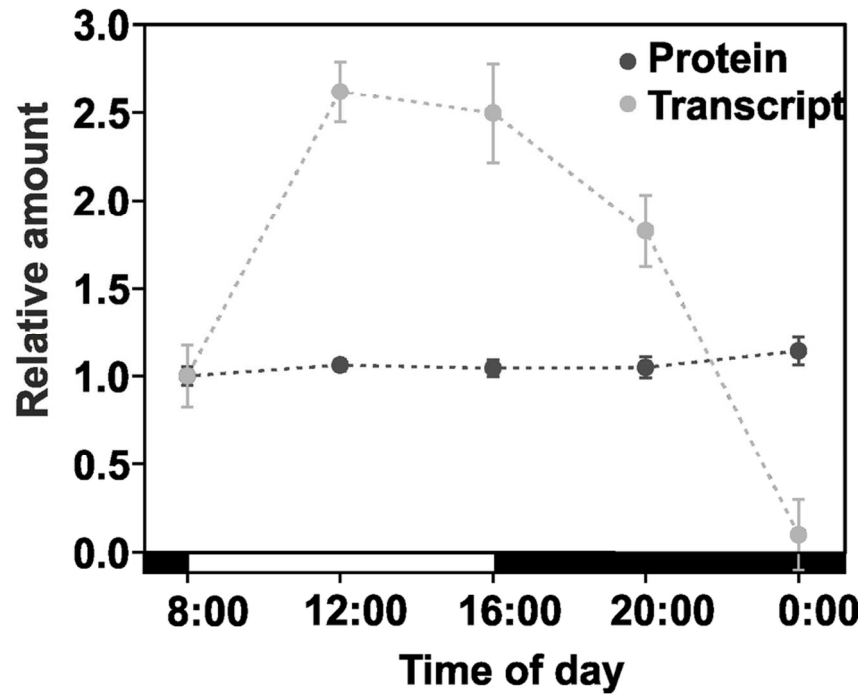


Figure 4. Expression and location of FNRL. (A) A representative Western blot showing the localization of FNRL. The proteins were separated using 12% SDS-PAGE with 6 M urea. D1 protein was used as a thylakoid marker. (B) *FNRL* gene and FNRL protein expression during day-night cycle. *FNRL* expression was studied with qRT-PCR (light grey) and protein amount with immunoblotting (dark grey). Black bar on the x-axis depicts the dark period of the day and white bar the light period.

82x113mm (300 x 300 DPI)